Available online at www.sciencedirect.com
SCIENCE DIRECT®
Nuclear Instruments and Methods in Physics Research A 496 (2003) 481–495
NUCLEAR INSTRUMENTS & METHODS IN PHYSICS RESEARCH Section A
www.elsevier.com/locate/nima

Linear electronics for Si-detectors and its energy calibration for use in heavy ion experiments

N. Taccetti, G. Poggi, L. Carraresi, M. Bini, G. Casini, R. Ciaranfi, L. Giuntini, P.R. Maurenzig, M. Montecchi, A. Olmi, G. Pasquali, S. Piantelli, A.A. Stefanini*

Dipartimento di Fisica dell'Università di Firenze, Istituto Nazionale di Fisica Nucleare, I-50125 Florence, Italy

Received 20 May 2002; received in revised form 9 September 2002; accepted 30 September 2002

Abstract

The design and implementation of linear electronics based on small-size, low-power charge preamplifiers and shaping amplifiers, used in connection with Si-detector telescopes employed in heavy ion experiments, are presented. Bench tests and "under beam" performances are discussed. In particular, the energy calibration and the linearity test of the overall system (Si-detector and linear and digital conversion electronics) has been performed with a procedure which avoids the pulse height defect problems connected with the detection of heavy ions. The procedure, basically, consists of using bursts of MeV protons, releasing up to GeV energies inside the detector, with low ionization density.

PACS: 29.40.W; 84.30.L

Keywords: Linear electronics; Silicon detectors

1. Introduction

This work originated in the frame of the experiment FIASCO [1] devoted to the systematic study of heavy ions collisions in the intermediate energy regime (10–40 A MeV) with the beams of the Superconducting Cyclotron of the Laboratori Nazionali del Sud (LNS-Catania). The experiment studies reactions which, typically, involve nuclei with $A \simeq 100$, with a target–projectile mass asymmetry of about 20%, in direct and reverse kinematics.

The detector set-up is based on Position Sensitive Parallel Plate Avalanche Counters (PS-PPAC) which determine the velocity vectors of primary (quasi-projectile and quasi-target) fragments, by measuring the time-of-flight (TOF) of the incoming particles and their impact point. These detectors cover a large fraction of the forward solid angle and those placed at small polar angles are backed by a matrix of 92 ΔE–E silicon detector telescopes of nominally 30 mm × 30 mm active area (ΔE manufactured by Canberra: 200 μm thickness; E manufactured by Hamamatsu: 500 μm thickness). These telescopes stop

*Corresponding author. Tel.: +39-055-457-2269; fax: +39-055-2269.
E-mail address: stefanini@fi.infn.it (A.A. Stefanini).

0168-9002/03/$ - see front matter
PII: S0168-9002(02)01767-9

the projectile-like heavy fragments and measure their energy. By combining this energy information with the TOF measured by the PS-PPAC, it is possible to deduce the secondary (post-evaporative) mass of the projectile-like fragment and to compare it with the primary mass, as deduced by the kinematic reconstruction of the reaction, in order to estimate the energy sharing in the reaction. Moreover, the ΔE–E configuration can be used to determine the charge of the projectile-like fragments, thus permitting a better characterization of the exit reaction channels.

Light charged particles (LCP) and intermediate mass fragments (IMF) emitted in these reactions are detected, except for the most forward angles, by 160 3-layers Phoswich telescopes. The three scintillators stack consists of 160 μm of BC404, 5 mm of BC444 and 30–50 mm of CsI(Tl).

The 92 ΔE–E silicon telescopes, placed at most forward angles, are backed by 50 mm CsI(Tl) scintillators. This configuration makes it possible to extend the detection of α-particles and IMF in the most forward cone.

This work reports on the design and performance of charge preamplifiers and shaping amplifiers, working in connection with the Si-detectors of the ΔE–E telescopes.

As shortly summarized in the following, linear electronics has been designed both for energy and for timing measurements.

The energy range, which must be covered in the experiment, is from MeV up to GeV (both for ΔE and E detectors) depending on the species of the detected particles which span a mass range from 4 to 100 amu. It is well known [2–4] that the detection of heavy ions in Si-detectors is characterized by significant plasma delay, extended collection time and charge recombination, generating pulse height defect (PHD) strongly dependent on charge, mass and total deposited energy. Those effects are associated with sizeable delayed and/or slower component in the current signals from the detectors; this component does not introduce any significant constraint on the design of the charge preamplifier, while suggesting the use of a signal integration technique, such as the one used, for instance, in connection with the INDRA multi-detector array [5]. However, since with increasing ionization density the charge recombination is more and more important, this prevents the possibility of obtaining, with heavy ion beams, accurate linearity performance and energy calibration of a Si-detector plus associated electronics. Therefore, in this work, accurate linearity and energy calibration measurements, in the range from MeV up to GeV, have been performed with 3 MeV closely packed protons. Furthermore, the so-obtained energy calibration can be used as an absolute reference for quantitative determination of the observed PHD (this will be the subject of a specific forthcoming paper).

As far as the TOF of different particles is concerned, the PS-PPAC provide the relevant information, except for low Z (<10), high-energy particles, whose detection efficiency becomes vanishingly small. In order to get the TOF of these particles also, the linear electronics of Si-detectors must have a fast preamplifier and a dedicated branch of fast amplification, which guarantee the necessary resolution (FWHM better than 1 ns) for TOF.

The work is organized as follows. Since the correct treatment of fast current waveforms is of particular importance in the design of a charge preamplifier to be used also for timing applications, Section 2 presents a detailed investigation of fast current waveforms generated by the Si-detectors of ΔE–E telescopes (this investigation makes use of the proton bursts technique, whose main characteristics are shortly reminded). In Section 3 the general guidelines of the design of charge preamplifier and shaping amplifier are introduced. Sections 4 and 5 concern with the implementation and test of charge preamplifier and shaping amplifier. Energy resolution measurements are discussed in Section 6 while Section 7 is dedicated to energy calibration and linearity measurements. Section 8 is devoted to short- and long-term tests of amplification stability. Results on timing resolution are reported in Section 9.

2. Current waveforms of silicon detectors

The knowledge of the current waveforms produced by the Si-detectors is an essential piece

of information for the design of the charge preamplifier. In fact, an estimate of the effectiveness of the feedback stabilizing action for a transient input of risetime t_{ri}, can be obtained if the risetime t_{rs} of the response of the amplifier to a step input is known [6]. To give an example pertinent to the present work, from the analysis of Ref. [6], it is possible to deduce that, almost independently of the detailed shape of the signals, for $t_{ri} = (1–10)t_{rs}$ the half value of a typical full stabilization of 10^{-2} is reached after $(3.5–0.5)t_{ri}$.

Taking all that into account, fast current waveforms produced by ΔE and E detectors have been analyzed in detail.

2.1. Measurement technique

Fast current waveforms from ΔE and E detectors have been obtained by bombarding the detectors with proton bursts generated by an electrostatic chopper installed on a beam line of the KN 3000 accelerator in Florence [7]. This technique makes it possible to drive the preamplifier, not through the test input, but directly from the detector in the same way as in case of heavy ion detection and, at the same time, to release large energy in the detector under conditions of negligible space charge effects. In fact, the detection of heavy ions is characterized by an increasing pulse height defect (up to several percent of the released energy) with increasing ion mass. For instance, using detectors similar to those of the present work, for Xe ions of ~ 1 GeV a pulse height defect larger than 5% has been measured.

Proton bursts, which directly impinge on the detector under test, have the following characteristics:

(1) Typical FWHM < 1.0 ns.
(2) Average number of protons per burst, from 1 to 500. In all the measurements with proton bursts, quoted in the following, protons of 3 MeV energy have been used. This corresponds to a mean energy per burst from 3 MeV to 1.5 GeV. It is to be observed that, for a given setting of the steady accelerator beam current, a distribution in the multiplicity of protons per burst is obtained, due both to short- and medium-term fluctuations of the current and to its intrinsic granularity. Therefore, during the same measurement, one simultaneously detects a largely variable number of protons per pulse, making it possible to obtain spectra with up to hundreds of peaks that are equally spaced in energy. In Ref. [7] the possibility of using his technique to perform in a direct way the test of the linearity of the detector plus preamplifier system has been already demonstrated.
(3) Repetition frequency from single shot up to 10^4 Hz.
(4) The transverse dimension of a burst impinging on the detector is typically of about 100 μm × 100 μm, corresponding to a mean distance among the individual proton tracks $\geqslant 1$ μm in any case. This suggests negligible space charge effects, at variance with the case of the dense columns of ionization which are typical of the heavy ion tracks.

Proton bursts of 0.5–1 GeV have been used to study the current waveforms of both ΔE and E detectors. As stated above, the proton energy was 3 MeV with a corresponding range in silicon of about 90 μm. The measurement of the current waveforms was made directly, as reported in Fig. 1, with a 2 G sample/s (400 MHz analog bandwidth) oscilloscope TDS380 (Tektronix) and in some cases with a 500 MHz oscilloscope LA354 (LeCroy).

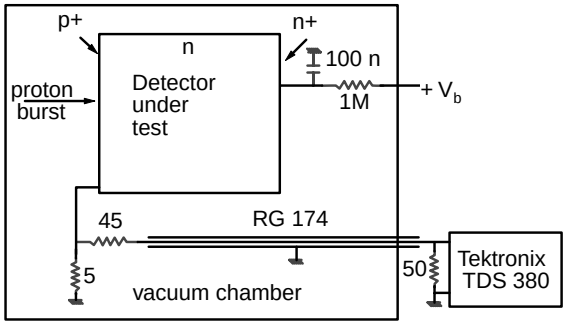

Fig. 1. Measurement technique of the current waveforms of ΔE and E detectors.

2.2. Current waveforms

As an example, in Fig. 2(a) a current pulse, generated by a burst of ~700 MeV released in an E detector (resistivity 5–12 kΩ cm, depletion voltage 100 V, operating voltage 120 V), is shown as a solid line while the corresponding calculated current pulse is shown as a dashed line. A sample of 10 detectors gave similar results.

A good agreement between measured and calculated pulses is found (both with respect to integrated current and total duration, while the detailed shapes are somewhat different) if the equivalent circuit of the detector contains, besides a current pulse generator $i(t)$ having in parallel the measured detector capacitance $C_D = 220$ pF, a series resistance $r_D = 5\ \Omega$, as shown in part (b) of the figure. The current $i(t)$, generated by the motion of electrons and holes inside the detector, has been calculated with the usual ingredients: dE/dx (taken from the tabulation of Ziegler et al. [8]), electric field of the ideal form $E(x) = (2V_d/W^2)x - (V_b + V_d)/W$ (where W is the detector thickness at the depletion voltage V_d and V_b is the applied bias voltage), relation among electron and hole velocities and the local electric field (taken from data of Ottaviani et al. [9]). The contribution to the current of every charge carrier is obtained by applying the Ramo's theorem.

A similar example is reported in Fig. 3 for a ΔE detector (resistivity 10–15 kΩ cm, depletion voltage 10–15 V, operating voltage 60 V). Again, in part (a) of the figure, the measured current pulse (solid line) and the corresponding calculated one (dashed line) are compared (also in this case a sample of 10 detectors gave uniform results). For these detectors, a damped oscillatory behaviour of the current pulse has been found, which has been verified to be independent of the length of the RG-174 cable as well as of different biasing layout and components. On the other hand, a rough calculation, based on the geometrical characteristics of the (microbonding) wire connecting the p^+ and n^+ surfaces of the detector to the output pins, suggests

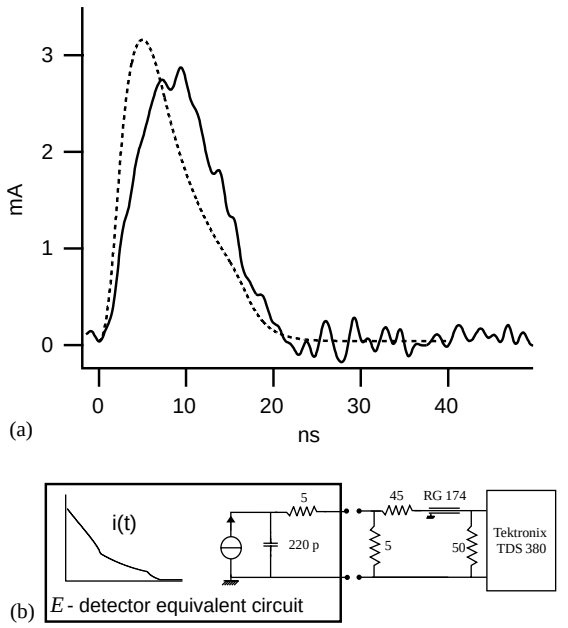

Fig. 2. Part (a) shows measured (solid line) and calculated (dashed line) current pulses generated by an E detector in response to a burst of total energy of ~700 MeV. In part (b) the equivalent circuit of the E detector, producing the calculated current pulse of part (a) is shown.

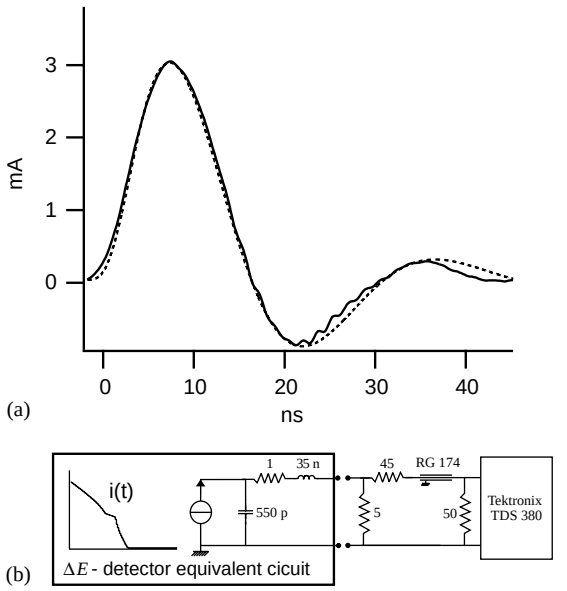

Fig. 3. Part (a) shows measured (solid line) and calculated (dashed line) current pulses generated by ΔE detector in response to a burst of total energy of ~700 MeV. In part (b) the equivalent circuit of the ΔE detector producing the calculated current pulse of part (a) is shown.

the presence of a series inductance of about 40 nH (this at variance with the case of E detector which has only one much more shorter connection).

Also in this case, starting from the calculated current pulse, a good agreement is found between measured and calculated waveforms, if the detector equivalent circuit shown in Fig. 3b is adopted. In particular, besides the measured detector capacitance $C_D = 550$ pF, this circuit contains a series resistance $r_D = 1\ \Omega$ and a series inductance $L_D = 35$ nH.

As a consequence of the previous observations, the equivalent circuits of Figs. 2(b) and 3(b) have been used to represent E and ΔE detectors as pulse generators feeding the front-end charge preamplifier. From these circuits, the current waveforms injected on an ideal virtual ground have been deduced and are shown in Fig. 4(a) and (b).

The time necessary to collect the 90% of the total charge comes out to be 15 ns for E detector, and ~ 70 ns for the ΔE detector, because of its oscillatory behaviour.

For the ΔE detector, Fig. 5 shows the calculated (dashed line) and measured (solid line) short

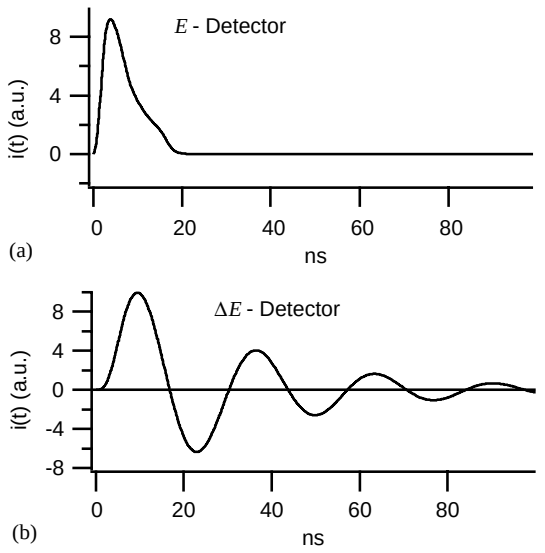

Fig. 4. Current waveforms generated on an ideal virtual ground by the equivalent circuits of E and ΔE detectors shown in Figs. 2(b) and 3(b). The time required to encompass the 90% of the total charge comes out to be ~ 15 ns for E detector and more than 70 ns for ΔE detector, because of the strongly oscillatory character of its current.

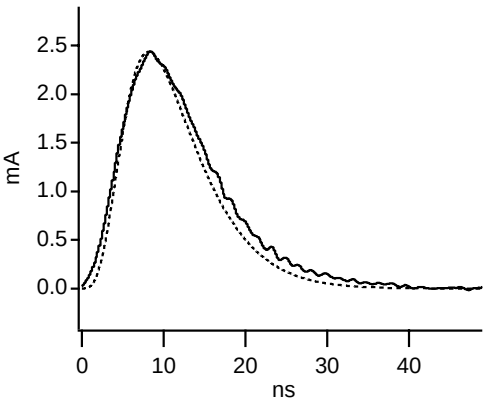

Fig. 5. Measured (solid line) and calculated (dashed line) current waveforms for ΔE detector, obtained by inserting a 14 Ω resistor in series to $r_D = 1\ \Omega$ resistor. In this way, when short circuited, the ΔE detector is critically damped. Energy of proton burst $\simeq 700$ MeV.

circuit current waveforms obtained inserting a 14 Ω resistor in series to r_D. In this way, the response is critically damped and the time to encompass 90% of the total charge reduces to ~ 20 ns. It is to be anticipated that the output waveforms of the home-made charge preamplifiers coupled to ΔE detectors showed a strongly oscillatory behaviour when the detector was directly coupled to the preamplifier and an almost monotonic fast response when a 14 Ω damping resistor was introduced. Results reported in the following refer, therefore, to ΔE detectors having in series a 14 Ω damping resistor.

3. Charge preamplifier and shaping amplifier design guidelines

3.1. Charge preamplifier

Taking into account the results of the preceding paragraph, further requirements, which have been considered in the design of the preamplifier, are the following:

(1) The preamplifier must be mounted in vacuum, as close as possible to its corresponding Si-detector; it must have small size and low power consumption.

(2) For a good TOF measurement of particles not efficiently detected by PS-PPAC, rise time should be as fast as feasible (typically $\leqslant 10$ ns).
(3) Long-term and short-term overall amplification stability (preamplifier + shaping amplifier + analog to digital conversion) better than $\pm 1\%$ and $\pm 0.1\%$, respectively, are demanded.
(4) Taking into account the expected energy range of the detected particles (up to 3 GeV) a reasonable conversion gain is 1 mV/1 MeV, that means a feedback integrating capacitor of 44 pF producing a maximum output amplitude of 5 V for a 5 GeV signal.
(5) The preamplifier must drive a 40 m-long RG58-U cable, terminated at the receiving end on its 50 Ω characteristic impedance; it implies that signals up to 100 mA have to be linearly transmitted.
(6) For the present application, because of the generally high value of the detected energy and of the presence of unavoidable effects deteriorating the energy resolution due to dead layers, channeling and PHD effects [2], a low electronic noise (at the level of tens of keV) is not of primary concern. However, high frequency (''series'') noise is to be kept to a minimum for a better timing performance.

3.2. Shaping amplifier

The design of the shaping amplifier was guided by the following considerations:

(1) For the sake of uniformity, 4096 channels QDC (CAEN VN1475) have been chosen for amplitude encoding of all type of detectors used in the experiment: PS-PPAC, Phoswich, Si-detectors. In connection with QDC, unipolar signals of finite duration permit an easier adjustment of width and starting time of the gate signal which determines the integration period.
(2) Both the broad energy range under measurement and the requirement of a quantization resolution better than 1% also at the lower energies, suggest that the amplifier be split into two channels differing by about a factor of ten in amplification and with independent gain setting.
(3) Energy signals must be linearly delayed (by about 500 ns) so that the corresponding QDC integrating gate signals be safely validated by the main trigger of the experiment.
(4) Long-term stability of the amplification as well as of the output baseline must be preserved.
(5) In some cases, a good time mark is of interest; this suggests the presence of a specific third channel of fast amplification and shaping for feeding the timing circuitry.

4. Charge preamplifier

4.1. Implementation

The requirement of low power consumption suggests to design a unipolar preamplifier (negative current input in the adopted configuration) keeping the steady current of the order of 2 mA in each active element. Moreover, in order to get a preamplifier with a fast settling time and a relatively high open loop gain, the chosen design relies on a short feedback loop of few active elements having a good gain–bandwidth product even at low current. It was therefore decided to use a low-noise bipolar transistor of moderate f_T as a first amplifying element and a reasonable choice came out to be the transistor MPS6521. As shown in Fig. 6, the amplifier is completed through a complementary pair (MRF904 and 2N4261) and a high β, high current transistor (2N2219A) used as an output stage of the emitter follower type. A few specific comments to the implementation follow. A separate bias voltage of the output ''power stage'' has been introduced, since it was found that in this way any residual cross talk among different preamplifiers was completely removed. Since unselected MPS6521 have been used, resistor R^* must be chosen to get the right biasing of the preamplifier, with no substantial current flowing in R_f. The feedback network is made with a NP0 capacitor $C_f = 47$ pF (conversion gain

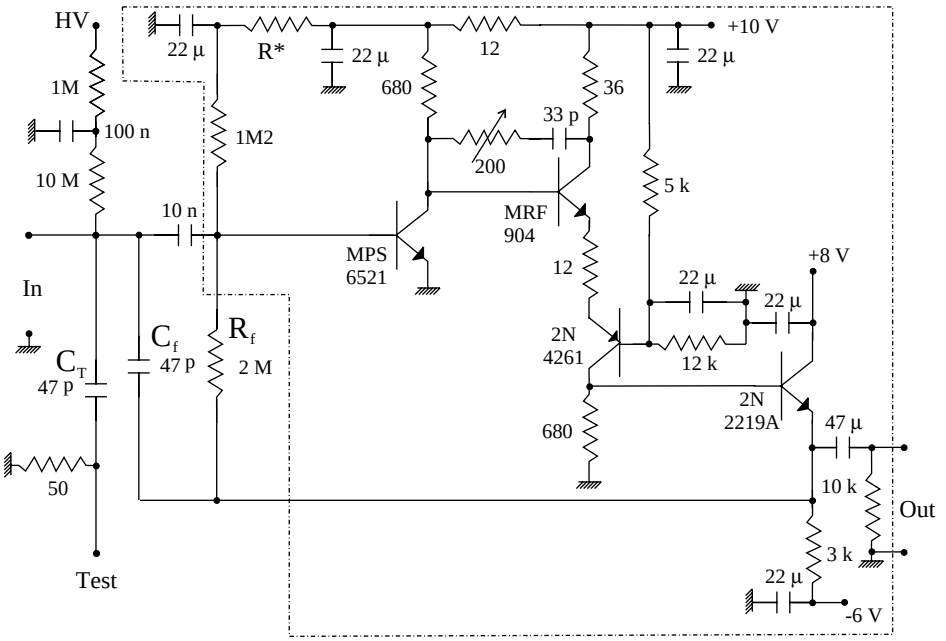

Fig. 6. Electrical scheme of the charge preamplifier. The basic amplifier is enclosed by dashed lines. Note the use of the bipolar transistor MPS 6521 as first amplifying element. Resistor R^* must be selected to have no nominal current flowing in the feedback resistor R_f.

0.94 mV/MeV) and a resistance $R_f = 2\ \mathrm{M\Omega}$. However, as it will be shown in the following, because of the small value of the input transistor resistance R_{iT} ($\sim 6\ \mathrm{k\Omega}$), the decay time constant comes out to be somewhat shorter than the usual product $C_f R_f$.

Moreover, because of the large value of the input capacitance C_{iT} (~ 300 pF) associated to the MPS6521, the response of the charge preamplifier to test input signals was very similar (with the same value of the trimming resistance of the frequency compensation group) for both types of detector, in spite of their substantially different values of capacitance.

Preamplifiers employed in the experiment FIASCO were mounted using discrete components on PC board of 30 mm × 70 mm. The overall cost for the laboratory is about 28 Euro each: it includes materials and the assembly.

4.2. Preamplifier tests

Power consumption turned out to be about 80 mW per preamplifier and it was verified that, also in continuous operation under a vacuum, no forced cooling was necessary. This significantly simplified the mechanics of the set-up.

A measurement of the open loop response of the basic amplifier (enclosed in the dashed lines in Fig. 6 and schematically drawn in Fig. 7(a)) has been performed. The measured response to the step input v_i ($t_r \sim 5$ ns) is shown as v_o ($t_r \sim 150$ ns) in part (b) of the same figure. To a good approximation, the rise time of v_o is characterized by a single time constant and, correspondingly, the (p-Laplace transformed) transfer function of the basic amplifier is reasonably well represented by the dominant pole relationship:

$$A(p) = -\frac{A}{1 + pT}$$

From signals like those reported in Fig. 7(b), taken from a sample of ten preamplifiers, the following "worst case" values were extracted:

$$A = 700, \quad T = 90\ \mathrm{ns}.$$

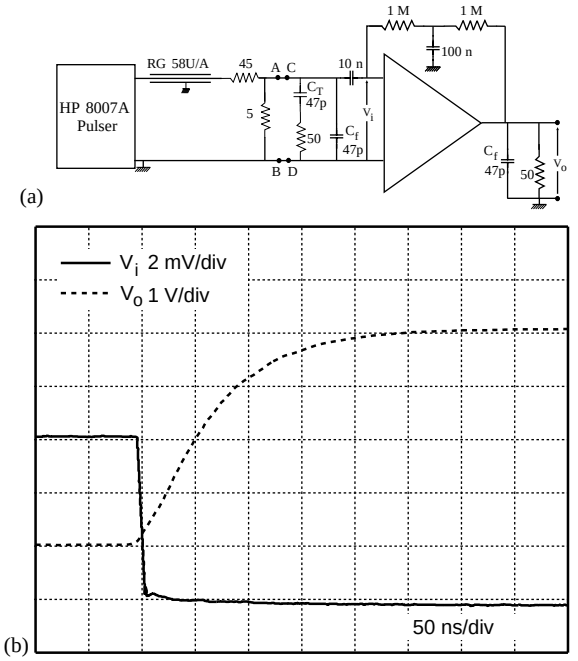

Fig. 7. (a) Configuration used to measure the response of the basic amplifier. (b) Input signal v_i measured with an active probe and a LECROY LA354 oscilloscope (amplitude 5.8 mV, rise time 5 ns) and the corresponding output signal v_o (amplitude 4.1 V, rise time 150 ns).

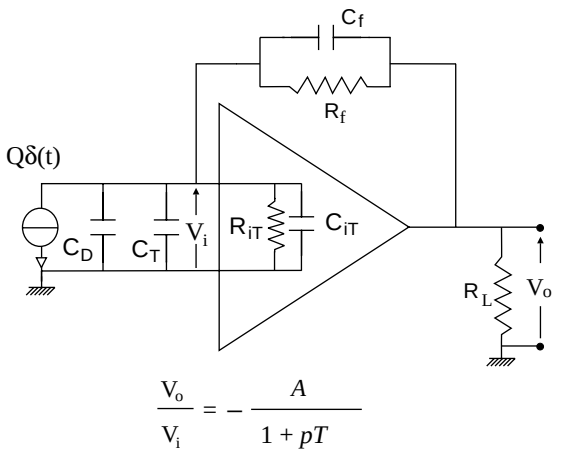

Fig. 8. Simplified scheme of the charge preamplifier used to deduce Eqs. (1) and (2).

Some general indication on the performance of the charge preamplifier can be obtained from the response of its simplified version (shown in Fig. 8) to an impulsive current $Q\delta(t)$.

The output signal has the expression:

$$v_o(t) = -Q\frac{A}{(C + AC_f + T/R_{iT})}(e^{-t/\tau} - e^{-t/\theta}) \quad (1)$$

and θ and τ ($\gg\theta$) are given by

$$\theta, \tau = \frac{2TC}{C + AC_f + T/R_{iT}} \times \left\{1 \pm \left[1 - \frac{4TC}{AC_f}\frac{1 + R_f/AR_{iT}}{C_f R_f}\right]^{1/2}\right\}^{-1}. \quad (2)$$

In expression (2) the plus sign in the curly braces is associated with the rise-time constant θ and the minus sign with the decay time constant τ.

Taking into account the measured values:

$$C = C_D(550 \text{ or } 220 \text{ pF}) + C_{iT}(300 \text{ pF}) + C_T(47 \text{ pF}) = 897(\text{or } 567) \text{ pF},$$

$$C_f = 47 \text{ pF}, \quad R_{iT} = 6 \text{ k}\Omega \quad \text{and} \quad R_f = 2 \text{ M}\Omega$$

one obtains the approximate solution:

$$v_o(t) \simeq -\left(\frac{Q}{C_f}\right)(e^{-t/\tau} - e^{-t/\theta})$$

with

$$\theta \simeq T(C/AC_f) \simeq 1.6-1.9 \text{ ns}$$

and a corresponding rise time

$$t_r \simeq 3.5-4.2 \text{ ns}$$

and

$$\tau \simeq R_f C_f(1 + R_f/AR_{iT})^{-1} \simeq 68 \text{ μs}.$$

It should be kept in mind that the present simplified analysis, while useful to get the right order of magnitude of both rise and decay times, is insufficient to make predictions about the presence and the amount of slew rate and/or of a damped oscillation in the output signal. Measured low and high level output signals, in response to step input signals (pulse generator HP 8131A), are shown in Fig. 9(a) and (b). The preamplifier was connected to an E detector and the rise time of a low level output signal ($\sim$120 mV) comes out to be $\sim$3.5 ns in agreement with the naive prediction, while the rise time of a high level output signal ($\sim$3.5 V) is $\sim$7 ns and shows an apparent slew rate. Similar results have been obtained with a ΔE detector. The

risetimes of the signals of Fig. 9 are the risetimes t_{rs} (introduced at the beginning of (Section 2)) of the output of the charge preamplifier to different step input amplitudes. If these rise times are compared with the input signal rise times t_{ri}, which can be extracted from Figs. 4(a) and 5, it is found that $t_{ri} \simeq$ (2–4)t_{rs}. Since the full stabilization is $\sim 10^{-2}$, the build up time of the stabilization to half of its final value is reached within (1.3–2.0)t_{ri}, that means $\simeq$20–30 ns. Moreover, numerical computations have been performed in order to estimate the variation ΔQ of the output charge Q, assuming an ideal behaviour of the shaping amplifier. Calculations based on input current waveforms like those reported in Figs. 4(a) and 5, suggest a percentage variation $\Delta Q/Q$ of 0.1% for a 10% variation of both amplification A and detector capacitance C_D, corresponding to a stabilization factor of 10^{-2}. In Fig. 10(a) the transient response to a proton burst of 1.7 GeV impinging on an E detector is shown, the rise time is $\simeq$12 ns and an overshoot of $\simeq$12% is apparent. However, it is to be noted that the corresponding damped oscillation, which extends over some tens of nanoseconds, is not expected to influence either the timing performance or the microsecond response; quantitatively its effect has been calculated to modify less than 1 part over 10^4

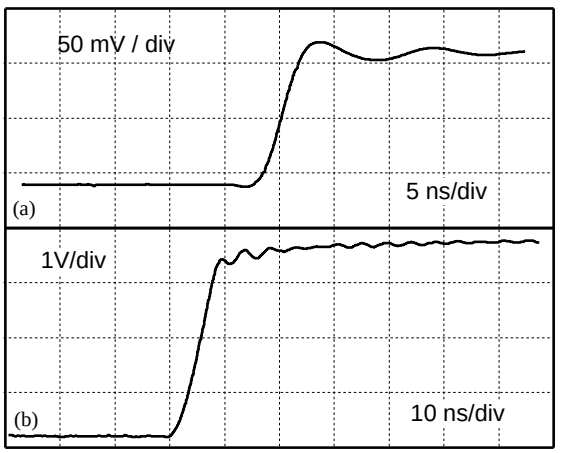

Fig. 9. (a,b) Output response of the charge preamplifier to fast pulses of amplitudes 120 mV and 3.5 V, respectively. The rise time of the 120 mV output is 3.5 ns and shows an 8% overshoot. The rise time of the 3.5 V output is 7 ns and exhibits a sizable slew-rate effect.

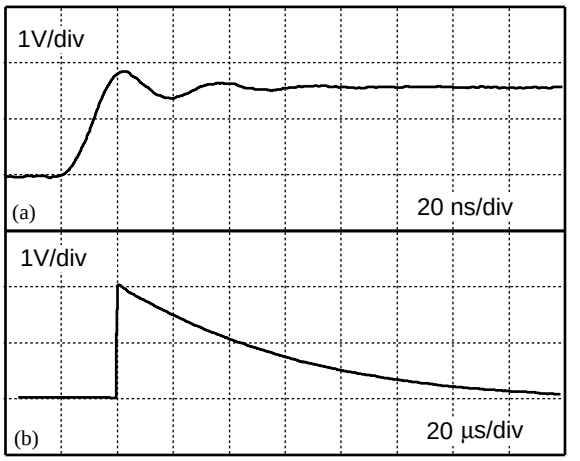

Fig. 10. Charge preamplifier connected with an E detector. In (a) an output pulse generated by a proton burst releasing an energy of 1.7 GeV in the detector is shown: the rise time comes out to be 12 ns and an overshoot of 12% is apparent. In (b) the long tail of a 2 GeV pulse is shown: the fall time is $\sim$62 μs.

the integrated value registered by the QDC. In Fig. 10(b) the exponential tail of a 2 GeV output signal is shown and its decay time constant is $\simeq$62 μs, again in substantial agreement with the previous calculation.

5. Shaping amplifier

5.1. Implementation

As shown in Fig. 11, the shaping amplifier consists of a fast and a slow branch. The slow branch, in turn, after a first common way of pole-zero cancellation, unipolar RLC wave-shaping and linear delay, splits into two section (both providing bipolar shaping, voltage to current conversion and clamping to ground of the output signal) completely identical apart from the amplification.

5.1.1. Fast timing amplifier

The positive input signal from the preamplifier is buffered by transistor T_1, differentiated with a time constant of 100 ns and amplitude limited by two back-to-back diodes. After amplification of 30 (transistors T_2–T_4), with signal amplitude again

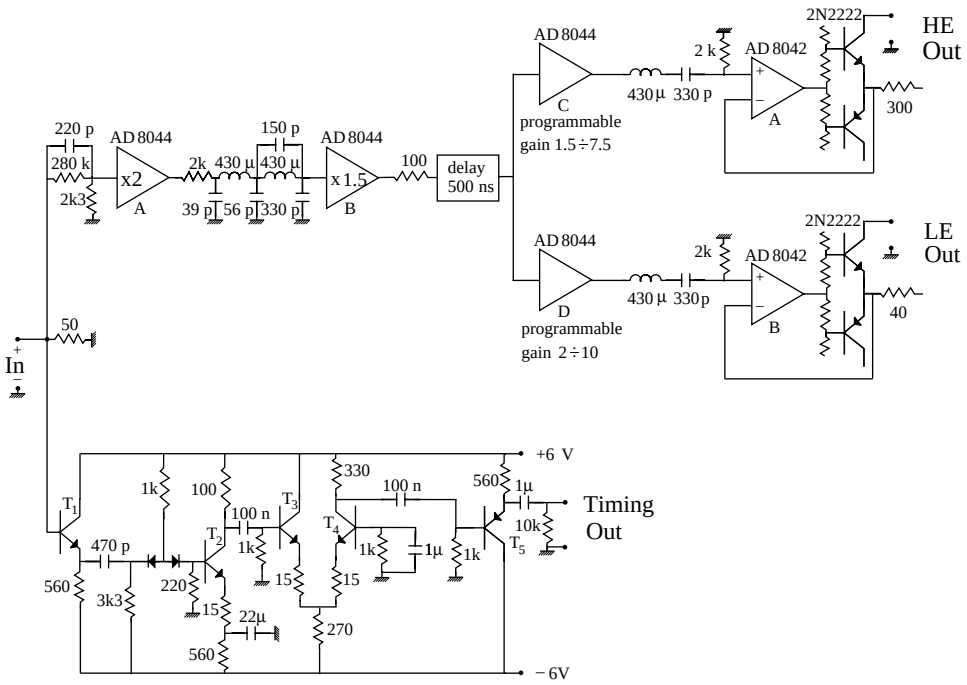

Fig. 11. Electrical scheme of the shaping amplifier.

limited to a maximum current of 10 mA in T_4, an emitter follower T_5 is used as an output stage. Examples of output waveforms for linear and current limited signals are shown in Fig. 12.

5.1.2. Slow shaping amplifier

After the pole-zero network (pole moved from 65^{-1} to 0.5^{-1} μs^{-1}), the signal is processed by the first part (substantially a low-pass filter) of a bipolar filter of the type devised in the sixties by Blankenship and Nowlin [10].

Two section (A and B, see Fig. 11) of a quad op-amp AD 8044 allow the proper impedance matching and introduce a gain of 3, while, in turn, the peak amplitude of the signal is reduced by the low-pass filter action by the same factor. Subsequently the signal is linearly delayed (500 ns) and then fed in parallel to the C and D section of the AD 8044, which have different, digitally programmable, gain settings. Their outputs are sent to two identical (quasi-critically damped) band-pass LCR networks, which produce bipolar signals having almost symmetric positive and negative lobes. The values of the components of

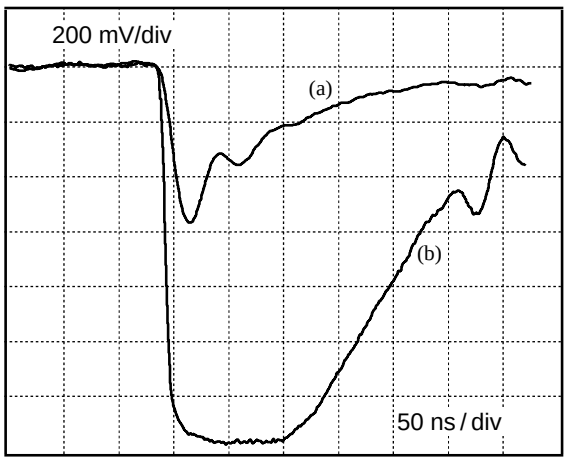

Fig. 12. Outputs of the fast (timing) branch of the amplifier induced by proton bursts releasing in the detector 20 MeV (a) and 1 GeV (b), respectively.

the pole-zero and of the filter networks have been selected to produce a bipolar signal reaching the peak of the first lobe after $\sim 1\,\mu s$ and the subsequent zero-cross after $\sim 2\,\mu s$. This choice

comes out to be a reasonable compromise among the different requirements coming from ballistic deficit, pile-up and noise.

The choice of bipolar signals was, in turn, recommended by two considerations:

(1) Long-term baseline stability can be substantially deferred to the last clamping stage which is operated in an intrinsically stable voltage follower configuration biased, in its steady state, just at the conduction limit.
(2) Precise clamping action on symmetrical bipolar signals with a fast return to the baseline is easier.

The bipolar signals are processed by two, structurally identical, active clamp circuits (each made by one section of an AD 8042 op-amp and two complementary transistors) similar to that devised for the INDRA multidetector [5]. The conversion gain of the amplifier is selectable in 8 steps in the range 2–10 nC V^{-1} for the high energy (HE) section and in the range 20–100 nC V^{-1} for the low energy (LE) section. As an example, a typical bipolar signal feeding the op-amp AD 8042 of the active clamp of the HE section is shown in Fig. 13(a); in part (b) the clamped output signal, as measured on a load of 50 Ω simulating the QDC input resistance, is also shown.

The devised solution makes use of two integrated linear chips and few discrete active elements. The amplifier is implemented with the surface mount technique on a daughter board of 5 cm × 7 cm and the quiescent power consumption is 1 W. In order to prevent even minute interferences among different amplifiers, caused by stray fields from lumped constant delay lines and shaping inductances, each daughter board has been enclosed in a box having 0.5 mm brass walls. For the same reason, input and output signals were sent via coaxial cables mounted on the mother board. Eight amplifiers per single CAMAC module are mounted and the whole shaping electronics of the Si-detectors is accommodated in a single CAMAC crate. The CAMAC bus is used to program the gain and to select the multiplexed output. The cost for the laboratory of an amplifying CAMAC module is about 700 Euro and is estimated as before.

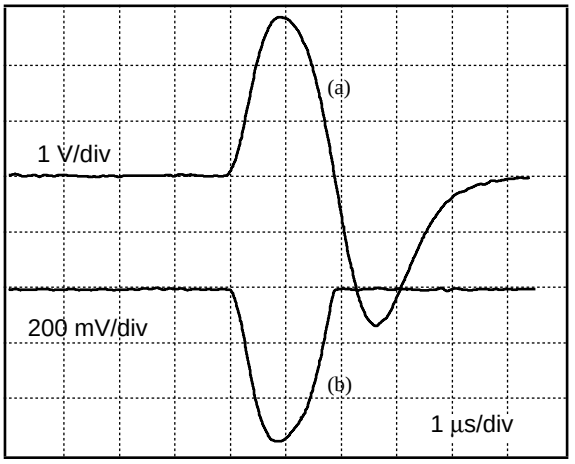

Fig. 13. HE section of the shaping amplifier. Typical waveforms, before (a) and after (b) the clamping circuit, are shown. The clamped pulse is measured on a 50 Ω termination, simulating the input resistance of a QDC.

6. Energy resolution measurements

As far as energy resolution is concerned, it is to be remembered that the shaping amplifier has been implemented with a HE and a LE channel with amplification typically differing by a factor of 10. In the last campaign of the FIASCO experiment, HE channels spanned an energy range up to 4 GeV and the quantization resolution was ≃1 MeV per channel. Measurements performed with a PB-4 pulse generator (Berkeley - Nucleonics) confirmed that the contribution from electronics to the energy resolution cannot be singled out in this case. In the same situation, the LE channels spanned an energy range of 400 MeV with a quantization resolution of ≃100 keV per channel. Typical FWHM of about 200–250 keV were measured partly coming from preamplifier (≃100 keV) and the most relevant part (≃200 keV) from the shaping amplifier, whose contribution was disentangled by driving the shaping amplifier directly with a PB-4 pulser. Moreover, specific measurements on a sample of 10 preamplifiers (followed by a 7611/L (Silena) spectroscopy amplifier and a 7420/G (Silena) ADC with a dispersion of ≃20 keV per channel) indicate FWHM values ranging from 60 to 150 keV. The large spread in the measured

FWHM is to be attributed to the first amplifying transistors (MPS6521) which were not selected.

7. Energy calibration and linearity measurements

Taking advantage of the proton bursts technique, it is possible to obtain an accurate energy calibration of the Si-detector and of the corresponding preamplifier in the range from MeV up to GeV energies and to get an absolute calibration of a high stability pulse generator which can be used as a reference for later measurements with heavy ion beams. This kind of calibration is planned to be used in future experiments performed by our group and it is to be expected to be a useful tool for a precise determination of the PHD effects of heavy ions in Si-detectors.

The proton bursts can also be used to measure the linearity of the overall system, including Si-detector, preamplifier, shaping amplifier and QDC, as described in the following.

A specific test concerned the linearity performance of the charge preamplifier coupled to an E detector.

In a first measurement, the non-linearity of a 7611/L amplifier (shaping time constant 1 μs, gain 2.5, integral non-linearity $\leqslant \pm 0.025\%$) and a 7420/G ADC (integral non-linearity $\leqslant \pm 0.025\%$) was tested in the range 60–8200 channels with a dispersion of 1 mV per channel. Signals from a PB-4 pulse generator (integral non-linearity $< \pm 0.005\%$) have been used and the deviations from linearity are reported in Fig. 14. The overall integral non-linearity comes out to be within $\pm 0.020\%$.

In a second measurement, the non-linearity of an E detector coupled to a home-made preamplifier followed by the 7611/L amplifier and 7420/G ADC was checked by bombarding the E detector with proton bursts. Having a mean number of 700 particles per burst, an energy range from 30 MeV to 3.8 GeV was explored. The measured multi-peaks spectrum is shown in Fig. 15(a). In Fig. 15(b) different energy regions are expanded: the worsening of the energy resolution with increasing burst energy arises from the correlated

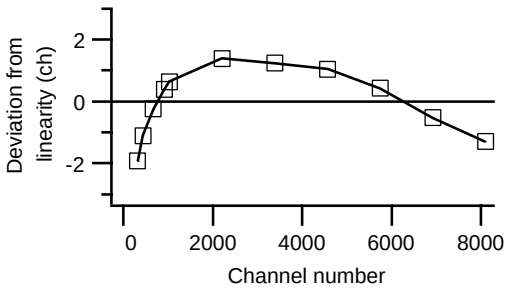

Fig. 14. Deviations from linearity of PB-4 pulse generator + 7611/L amplifier + 7420/G ADC; the integral non-linearity in the range 60–8200 channels is $\pm 0.020\%$.

energy fluctuations of the individual protons (accelerator HV ripple and medium-term stability are estimated to give a FWHM of ~ 1 keV per particle).

The trend of the deviation from linearity, reported in part (c) of the figure is rather different from that of Fig. 14 and also the integral non-linearity $\pm 0.045\%$ is about a factor of 2 larger than that reported in the same figure. Therefore, it is reasonable to attribute to the E detector plus preamplifier a non-linearity of $\pm 0.045\%$ in the energy range 30 MeV–3.8 GeV. Moreover, as explained in Section 2.1, if negligible non-linearity effects associated with the Si-detector excitation are assumed, the non-linearity behaviour, shown in Fig. 15(c), can be attributed to the not fully stabilized variation (with the signal amplitude) of the transistors parameters.

Finally the results obtained with a standard chain of the FIASCO experiment are reported. In this measurement, the 7611/L amplifier was replaced with a home-made shaping amplifier and a 4096 channel QDC model VN1475 was used. In Fig. 16(a) the sum of three energy spectra collected with the E detector is reported. The spectra are in partial overlap for an easier counting of the individual peaks starting from the single proton peak and span an energy range of ~ 2.4 GeV. This limit was imposed by the maximum proton energy (3 MeV), which is also the energy difference between consecutive peaks. In order to distinguish clearly two adjacent peaks a conversion gain no larger than 600 keV per channel must be used. All this is apparent in part

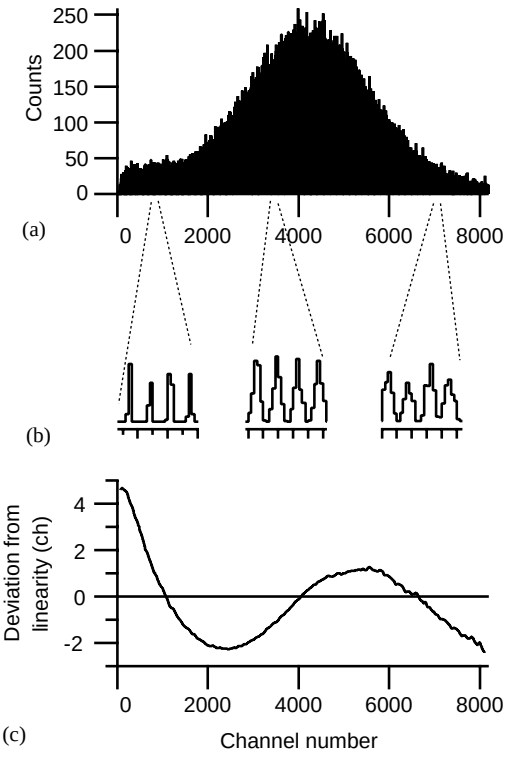

Fig. 15. (a) Energy spectrum recorded by the E detector plus charge preamplifier followed by 7611/L amplifier and 7420/G ADC. The spectrum spans an energy region from $\simeq 30$ MeV to $\simeq 3.8$ GeV. (b) Details of the spectrum in different energy regions. The worsening of the resolution with increasing energy is discussed in the text. (c) Deviations from linearity are shown; the integral non-linearity is $\pm 0.045\%$.

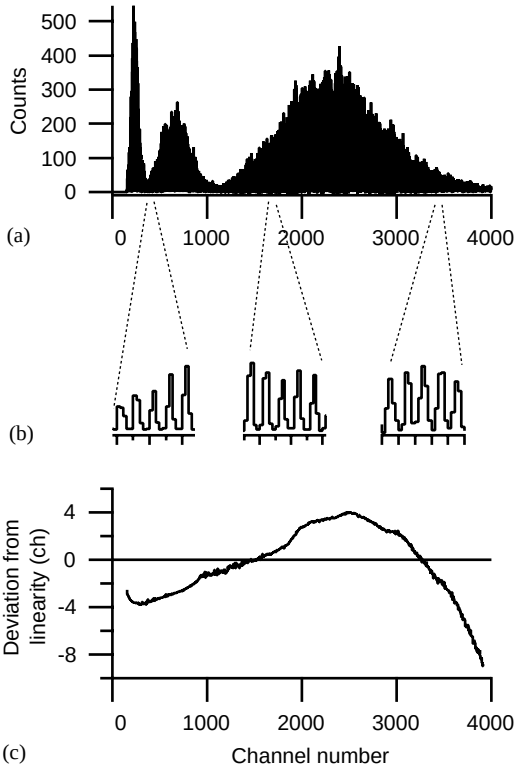

Fig. 16. (a) Energy spectrum recorded in 3 successive irradiations with bursts containing an average number of 15, 150 and 500 protons. (b) Details of different energy regions. (c) Deviations from linearity are shown. The integral non-linearity in the range 3 MeV–2.4 GeV comes out to be $\pm 0.15\%$, mainly concentrated in the range 2500–4000 channels.

(b) of the figure in which details of different energy regions are given.

The deviations from linearity are shown in part (c) of the figure. The general trend of the deviations looks different from that of Fig. 15(c) and also the integral non-linearity ($\pm 0.15\%$) comes out to be more than 3 times larger than that of the charge preamplifier and in principle it can be attributed both to the shaping amplifier and to the QDC. In fact, a specific measurement, where "rectangular pulses" (rise time 50 ns, flat top 500 ns, decay time 500 ns) from PB-4 pulser were sent directly to the QDC, clarified that the dominant contribution to the non-linearity was given by the QDC itself and that it was mainly concentrated in the range 2500–4000 channels.

8. Amplification stability measurements

To test the amplification stability of the charge preamplifier at short time, the centroid of a pulser peak was measured with the E detector connected to the preamplifier input without and with an additional capacitor of 22 pF ($= 0.1\ C_D$). In the presence of the additional capacitor, a centroid shift toward smaller amplitudes of 0.08% was found, in agreement with the calculation of Section 4.2.

Long-term amplification stability of the overall system was checked during the measurements made at LNS with beams of ^{93}Nb and ^{116}Sn. The elastically scattered ions deposit comparable energy in ΔE and E detectors, but, due to

channeling effects, the energy partition between ΔE and E detectors fluctuates so that scarce information about stability can be extracted from the individual detector. On the contrary, it has been possible to measure the sum energy ($\Delta E + E$) to an accuracy of better than 1 MeV, and its stability was followed for runs lasting typically 2–3 days. As an example, Fig. 17 presents the results obtained with 6 ($\Delta E + E$) telescopes in the measurement of the elastic scattering peaks produced by a 3.5 GeV ^{116}Sn beam on a ^{93}Nb target. From the data of Fig. 17, a maximum overall instability within $\pm 0.2\%$ in 3 days is found (to which also the energy instability of the beam can give a contribution). In any case, since during these measurements room temperature varied from 23°C to 27°C, one conservatively finds a maximum temperature sensitivity of the overall system of $\pm 0.05\%/^{\circ}$C.

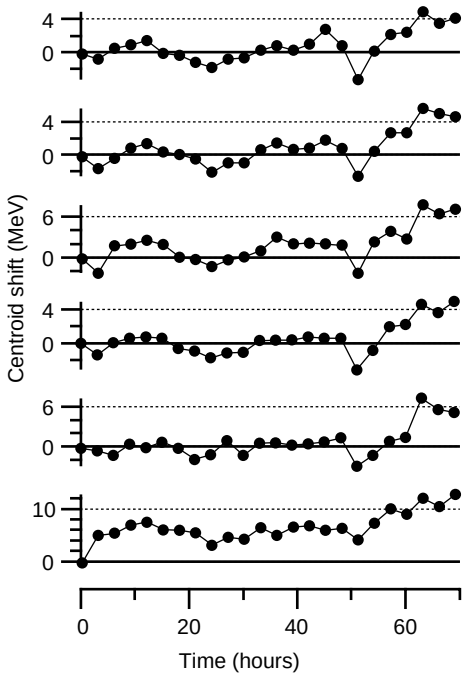

Fig. 17. Results of a 72 h stability run for a sample of six ($\Delta E, E$) telescopes. The centroid shifts of the elastic scattering peak, produced by a 3.5 GeV beam of ^{116}Sn, are reported with respect to the centroid position in the first measurement. Errors are smaller than the size of the symbols.

9. Timing performance

As underlined in Section 1, one of the applications of the Si-detectors was to measure with reasonable resolution (FWHM < 1 ns) the TOF of low Z (< 10), high-energy particles, releasing in the detectors energies in the range 30–300 MeV. To this purpose, particular attention was paid to the design of a fast preamplifier with little high frequency noise and a fast shaping branch of amplification with a fast recovery time also in case of extreme overload conditions.

Since the detection of low Z, high-energy particles is accompanied by negligible plasma effects, a study of the time resolution as a function of the released energy, performed with proton bursts, comes out to be meaningful and relatively easy.

In more detail, a signal derived from the voltage transition of the electrostatic deflector, generating the proton burst, is used to start a Time-to-Digital Converter (TDC). This signal is known to be accurate to better than 100 ps from separate, specific measurements. The stop to the TDC is given by the timing signal from the fast branch of the shaping amplifier (fed by a E detector plus preamplifier) after processing by a discriminator used in the Leading Edge Trigger (LET) mode. This technique, which does not compensate for different signal amplitudes is, however, well suited to single out the intrinsic noise limit to the time resolution. A reasonable value of the LET threshold come out to be about 10 times higher of the rms value of the fast amplifier noise output.

Data acquisition was performed with a standard, two-parameter, coincidence technique: the energy of the proton burst and its corresponding delay time with respect to the deflector voltage transition were recorded.

To give an example, in Fig. 18(a) a scatter plot of the delay time distribution measured by the TDC is reported as a function of the energy deposited in the Si-detector by the proton bursts, in the range 9–350 MeV. In this range, the amplitude-dependent walk of the delay time distribution is found to be ~ 16 ns, consistent with the combination of the LET threshold setting and of the rise time of the signals. Part (b) of the figure presents the FWHM of the delay time distribution

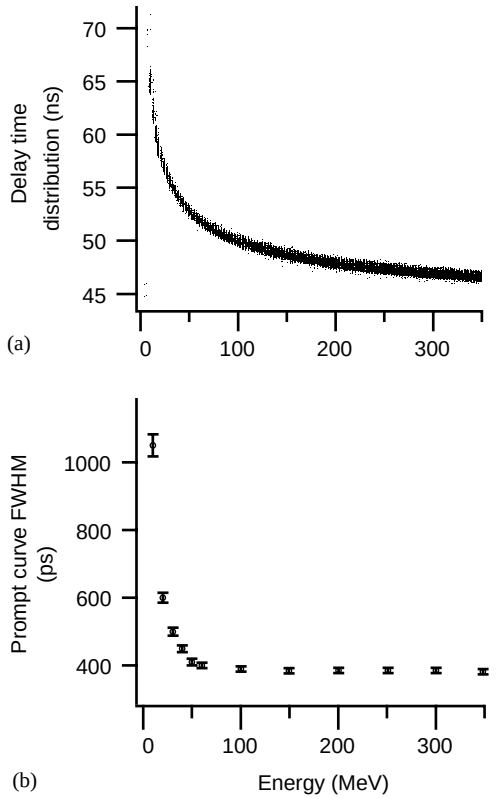

Fig. 18. (a) Scatter plot of the delay time distribution reported as a function of the energy released in the detector by the proton bursts. (b) FWHM of the delay time distribution reported for different energies released in the detector. For energies higher than 50 MeV the FWHM levels around a value of 400 ps.

for a sample of bursts of different proton numbers, exploring again the energy range 9–350 MeV. The FWHM values vary from ~ 1 ns to ~ 500 ps in the range 9–30 MeV and almost level off around the value of 400 ps for energies higher than 50 MeV.

These results confirm the possibility of measuring with sufficient accuracy the TOF of low Z, high-energy particles releasing in Si-detectors energies higher than 30 MeV.

10. Conclusions

The design, implementation and the performed extensive tests of linear electronics for Si-detectors employed in heavy ion experiments have been presented. Special attention has been devoted to design very low power preamplifiers, however capable of handling correctly fast signals [6]. As far as shaping amplifiers are concerned, a specific fast branch has been introduced for timing measurements. The slow branches are based on a network [10] which generates bipolar signals with a high degree of symmetry, followed by an active clamp circuitry which prepares unipolar signals for QDC's integration.

Concerning the energy measurements, overall non-linearity within $\pm 0.15\%$ in the range 3 MeV–2.4 GeV and under beam long-term stability within $\pm 0.05\%/^{\circ}$C have been obtained, while maintaining a sufficient energy resolution (FWHM < 250 keV).

Moreover, taking advantage from the low ionization density created by the proton bursts inside the detector, absolute energy calibration in the range 3 MeV–3.8 GeV have been obtained in a straightforward way. Based on similar calibrations, quantitative study of the PHD produced by heavy ions in Si-detectors are in progress.

Concerning the timing performance, the proton burst technique made it possible to also find that the intrinsic resolution is better than 500 ps in the range 30–350 MeV of energy released by high-energy, low Z particles. This demonstrates the feasibility of sufficiently accurate TOF measurements with Si-detectors coupled to the electronics presented in this work.

References

[1] S. Piantelli, et al., Phys. Rev. Lett. 88 (2002) 052701.
[2] G. Pasquali, et al., Nucl. Instr. and Meth. A 405 (1998) 39.
[3] G. Tabacaru, et al., Nucl. Instr. and Meth. A 428 (1999) 379 and references quoted therein.
[4] G. Pausch, W. Bohne, D. Hilsher, Nucl. Instr. and Meth. A 337 (1994) 573.
[5] J. Pouthas, et al., Nucl. Instr. and Meth. A 369 (1996) 222.
[6] K. Fränz, H. Paucksch, Nucl. Instr. and Meth. 27 (1964) 125.
[7] N. Taccetti, et al., Nucl. Instr. and Meth. B 188 (2002) 255.
[8] J.F. Ziegler, J.P. Biersack, U. Littmark, The Stopping and Range of Ions in Solids, Pergamon Press, New York, 1996.
[9] G. Ottaviani, et al., IEEE Trans. Nucl. Sci. NS-22 (1975) 192.
[10] J.L. Blankenship, C.H. Nowlin, New concepts in nuclear pulse amplifier design, 10th IEEE Symposium on Scintillation and Semiconductor Counters, Washington, DC, March 1966.